Additive Manufacturing 35 (2020) 101358

Contents lists available at ScienceDirect

Additive Manufacturing

journal homepage: www.elsevier.com/locate/addma

Precipitation printing towards diverse materials, mechanical tailoring and functional devices

Ruowen Tu[a], Ethan Sprague[b], Henry A. Sodano[a,b,c,*]

[a] Department of Aerospace Engineering, University of Michigan, Ann Arbor, MI, 48109, USA
[b] Department of Material Science and Engineering, University of Michigan, Ann Arbor, MI, 48109, USA
[c] Department of Macromolecular Science and Engineering, University of Michigan, Ann Arbor, MI, 48109, USA

ARTICLE INFO

Keywords:
Precipitation printing
Solution printing
Mechanical tailoring
Functional devices

ABSTRACT

Additive manufacturing allows for the fabrication of complex structures which are hard to achieve through conventional machining, extrusion, injection molding or blow molding processes. Current additive manufacturing methods for polymers, such as vat photopolymerization, powder bed fusion, material extrusion and binder jetting, still have limitations on the types of polymers that can be 3D printed. Recently, a novel solution-based polymer additive manufacturing method, termed precipitation printing, is developed which is based on the solubility of the polymer being printed in two mutually miscible solvents. In this work, the precipitation printing technique is further developed to expand the range of applicable materials, towards different thermoplastics (poly(vinylidene fluoride) (PVDF) and poly(methyl methacrylate) (PMMA)), thermoset rubber (acrylonitrile butadiene rubber (NBR)) and polymer nanocomposites (multiwalled carbon nanotubes (MWCNTs)-PVDF). The printing process is rapid and enables the realization of large structures with complex geometries as well as printing at a higher resolution than the material extrusion method, while also allowing the fabrication of micro-scale structures with greater than 100 μm resolution. Porosity and mechanical property tailoring of the precipitation printed materials are achievable through the control of process parameters, such as solvent/non-solvent pair selection, salinity of the non-solvent and printing temperature. In addition, the successful demonstrations of a directly 3D printed NBR check valve and a MWCNTs-PVDF strain gauge indicate the great potential for precipitation printing as a promising one-step process for the production of functional devices.

1. Introduction

Additive manufacturing (3D printing) defines a group of fabrication techniques that are capable of manufacturing complex parts layer by layer without geometric restrictions encountered in conventional manufacturing techniques [1]. With the development of computer-aided design (CAD) and computer-aided manufacturing (CAM), additive manufacturing provides nearly unlimited design freedom and manufacturing convenience for industry [2]. Recent advances in additive manufacturing have changed it from merely prototyping models to directly manufacturing final products [3]. Polymers are one of the most widely used materials in industry and have garnered significant attention in the additive manufacturing field over the last 30 years [4]. Common additive manufacturing methods for polymers include laser-based techniques such as vat photopolymerization and powder bed fusion, extrusion-based techniques such as material extrusion, as well as binder-based technique, *e.g.* binder jetting [5,6]. Recently researchers have developed laboratory additive manufacturing methods with pneumatic controlled extrusion or dispensing of materials, such as direct ink writing [7]. However, there are still limitations on the types of materials that can be fabricated through these well-developed methods. For example, vat photopolymerization requires a photocurable polymer resin which is usually expensive [8], and direct ink writing requires a fluid gel or ink with suitable viscosity for printing [7]. Among all these polymer additive manufacturing methods, material extrusion is currently the most commonly used approach for polymers [9] due to its short cycle time, high-dimensional accuracy, low cost and convenient integration with different CAD software [10]. Standard polymers for material extrusion are acrylonitrile butadiene styrene (ABS), polylactic acid (PLA), polycarbonate (PC), polystyrene (PS) and polyethylene (PE), and they are commonly used for low cost material extrusion printers designed to print simple models. Material extrusion has also been used to print thermoplastic based composite filaments to improve the strength of the material, such as short glass fiber reinforced ABS

* Corresponding author at: Department of Aerospace Engineering, University of Michigan, Ann Arbor, MI, 48109, USA.
E-mail address: hsodano@umich.edu (H.A. Sodano).

https://doi.org/10.1016/j.addma.2020.101358
Received 17 March 2020; Received in revised form 13 May 2020; Accepted 25 May 2020
Available online 30 May 2020

[11], carbon fiber reinforced ABS [12], iron/ABS and copper/ABS composites [13].

Polymer nanocomposites for functional structures, like strain gauges can also be printed by material extrusion [14]. Despite its broad reach and ubiquity, the material selection for extrusion is still limited by the melting process, and only neat thermoplastics or thermoplastic based composites can be manufactured. For polymers with a high melting point (*e.g.*, polyetheretherketone (PEEK)), or those that decompose below their melting point, as well as those with properties stable only below a certain temperature (*e.g.*, piezoelectric β phase of PVDF [15]), material extrusion is not an acceptable technique. In addition, material extrusion is often subject to deformation through warping of the part which results due to thermal stress [16,17], and can lead to the detachment of the printed structure from the bed platform during printing even if the bed is heated.

To overcome the limitations of material extrusion, researchers have developed solution-based additive manufacturing methods, which can be applied to any polymer soluble in certain solvents. With solution-based methods, the range of polymers available for additive manufacturing has been greatly expanded. Solvent-cast 3D printing or direct ink writing is one of the most commonly used solution-based methods. With this method, a polymer solution is extruded out of a nozzle under precise pneumatic control, and the polymers then solidify through the rapid evaporation rate of the solvent on a hot bed substrate [18]. This printing method has been successfully applied to print small scale functional material structures such as piezoelectric PVDF nanocomposites [19] and PLA/MWCNT nanocomposite [20]. However, since the solvent evaporation rate decreases as the nozzle moves away from the heated substrate, it is difficult to print large structures. Wet spinning, another newly developed solution-based additive manufacturing method in the biomedical engineering field has been applied to fabricate scaffolds for cell growth and injects a polymer solution directly into a coagulation bath with a poor solvent to solidify polymer fibers [21–23]. This technique is suitable for printing fine scaffolds with wet spun fibers, but only biomaterials, such as polyhydroxyalkanoates (PHAs) or poly(ε-caprolactone) (PCL) have been demonstrated. In addition, the requirement that the printed parts forming within fibers or scaffolds results in limitations for this printing method. Recently, a novel solution-based additive manufacturing technique which utilizes the rapid precipitation of the solute when the printing solution is exposed to a reservoir of a poor solvent has been developed to expand the range of applicable materials. Similar to the process of wet spinning of fibers, or bioplotting which is an additive manufacturing technique commonly used for biological materials [24,25], the reservoir draws solvent reducing solubility of the solute leading to rapid precipitation. Karyappa et al. introduced this technique which was termed immersion precipitation 3D printing (*ip*3DP) to 3D print porous materials for energy storage, catalysis and biotechnology, and they have demonstrated the capability of printing a wide range of thermoplastics using this technique [26]. In addition, with this precipitation printing, internal porosity of the prints could be controlled by varying the vapor pressure and the ink viscosity.

In this research, the potentials and applications of the precipitation printing are further investigated. Materials made using this technique are self-supporting and capable of complex geometries with high accuracy. The range of materials could be printed using precipitation printing is extended from thermoplastics to thermoset rubbers and polymer nanocomposites, which is demonstrated through the printing of poly(vinylidene fluoride) (PVDF), poly(methyl methacrylate) (PMMA), acrylonitrile butadiene rubber (NBR) and multiwalled carbon nanotubes (MWCNTs) - PVDF nanocomposites. The scale of the prints could be comparable to those structures made by material extrusion method, but it could also reach a high printing resolution for microstructures. Compared with material extrusion or solvent-cast 3D printing, the precipitation printing technique does not require material melting or solvent evaporation, which allows for room temperature printing and removes the safety risks associated with the volatilization of the solvent. Moreover, using a setup similar to direct ink writing, the precipitation printing technique requires relatively low equipment and printing cost. In this work, the printing solution preparation process and the equipment setup are explained in detail. Mechanical properties of a range of printed materials are characterized, and the control of printing parameters indicates the potential of porosity and mechanical property tailoring. Several directly printed devices are also demonstrated to show the one-step manufacturing of functional devices using precipitation printing.

2. Experimental setup

2.1. Printing solution preparation

To prepare the solution for the precipitation printing, a suitable solvent for the polymer is used to dissolve the polymer and disperse the filler in the case of polymer nanocomposites. The choice of solvent will therefore be dependent on the polymer to be printed, however for this study we have used *N,N*-dimethylformamide (DMF) (ACS certified, Fisher Chemical) for PVDF and acrylonitrile butadiene rubber (NBR), and Acetone (ACS reagent, Sigma-Aldrich) for PMMA. The polymer is first dissolved in the solvent through a combination of shear mixing and sonication until a uniform solution is. A non-solvent for the polymer to be printed is then selected such that the solvent for the polymer is miscible and can surround the print bed. For the polymers used in this study, water or ethanol act as suitable precipitation medium. Each polymer-solvent pairing is chosen based on the solubility of the polymer in the solvent, and the way the polymer solution acts when it is exposed to the non-solvent in the reservoir. The suitable polymer-solvent pair and the weight fraction used to print each material are listed in the **Supplementary Materials**. The weight fraction of solute in the printing solution ranges from 15 % to 25 % but is dependent on the particular polymer being printed and is selected to ensure both high precipitation rate and suitable viscosity of the printing solution.

2.2. 3D printing setup and process

The custom-designed 3D printer is based on a Cartesian gantry system (AGS1500, Aerotech), which is shown in Fig. 1a. The printing substrate for all precipitation prints was a flat glass plate inside a non-solvent reservoir, and a thin film of the same solute polymer was doctor bladed on the glass plate to enable adhesion with the substrate through diffusion bonding. To improve the adhesion of the doctor bladed film to the glass plate, the film was first allowed to solidify from solution at 100 °C, then heated up to a temperature above the melting point of the polymer and then allowed to cool down slowly to room temperature. The printing solution was loaded into a 10 mL syringe with a stainless-steel dispensing needle. The needle size ranged from 24-gauge (305 μm) to 30-gauge (150 μm) for different printing solutions and to achieve variation in the print speed and resolution. Pressure was applied to the solution between 1.0 psi (6.9 kPa) to 30.0 psi (207 kPa) using a high precision dispenser (Ultimus V, Nordson EFD) such that a constant flow rate was obtained. Large variances in the pressure for a given solution concentration and printing speed combination can lead to printing errors such as coagulation in the needle, inability to print multiple layers due to layer thickness and surface issues, or insufficient inter-layer or bed adhesion.

Needle toolpaths for precipitation prints were made using the open-source extruder toolpath software (Slic3r) from. STL files made in CAD drawing software (SolidWorks, Dassault Systèmes). The needle printing speed was set between 5 and 12 mm/s, and the layer height was varied between 0.03 and 0.10 mm based on the desired resolution of the final 3D structure. During printing, the needle tip remained in the non-solvent until the print was finished. Furthermore, the pressure applied to the solution in all prints was never paused during a print, even during

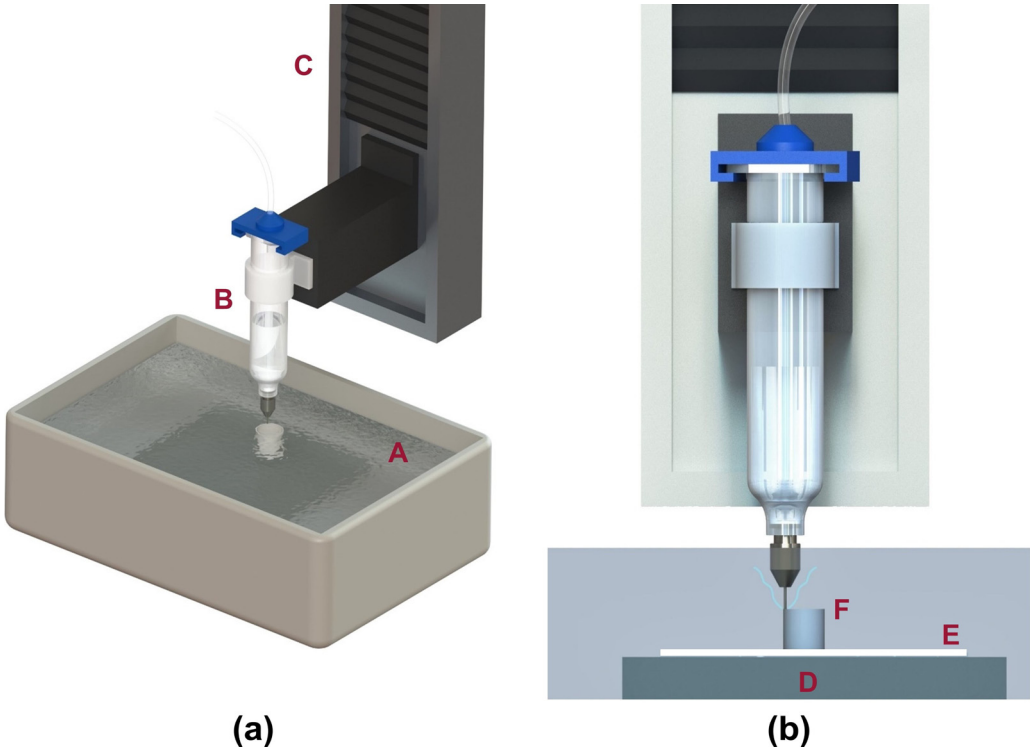

Fig. 1. (a) 3D printing setup overview. A: Reservoir filled with the non-solvent. B: Syringe with printing solution. C: Cartesian gantry system (only the Z stage is shown in this figure). (b) Schematic of the printing process. D: Glass substrate. E: Doctor bladed film. F: Printed sample.

the non-printing movement steps to prevent clogging of the dispensing needle due to precipitation of the polymer inside the needle tip. The continuous flow of the print solution did not significantly affect the quality of the final prints, as the non-printing movements were set at much higher velocities (60 mm/s) than that of the printing movements, thus features from the non-printing movements were much thinner than those made at printing speed.

The precipitation printing technique is based on the different solubility of the polymer in two mutually miscible solvents. Because the solvent is miscible in the non-solvent while the solute polymer is not, as the solution leaves the needle the solvent begins to diffuse away from the polymer, and the polymer precipitates and solidifies. If the needle dispenses the solution close to the previous layers, the solution appears to dissolve the printed polymer, resulting in bonding between each layer. What is left is a porous solid that is printed layer by layer. To prevent the print from sticking irreversibly to the film substrate, the first two layers of all prints are printed as low infill percentage raft layers. An optional hotplate/stirrer can be used to heat the reservoir to a slightly elevated temperature to increase the solvent diffusion rate if high printing speed is desired. A magnetic stirrer can also be used to accelerate the solvent diffusion process for some specific applications. Once printing is complete, prints were left in the reservoir for at least an hour to allow any left solvent to diffuse out of the polymer. Samples were removed from the reservoir, had their raft layers removed and dried under vacuum overnight.

3. Results and discussion

3.1. Diverse applicable materials and structure scales

The precipitation printing technique is capable of printing a wide range of thermoplastics reported by Karyappa et al., [26]. In this research, more thermoplastics of different properties were tested to expand the range of printable materials. Fig. 2a shows an example of precipitation printed PVDF chess pieces and demonstrate high resolution and uniform structure over the build height. The nozzle dimensions can be varied to achieve a desired build, with larger diameter leading to a faster build and a smaller diameter leading to higher resolution. For PVDF a 26-gauge needle (254 μm) was used to 3D print with high resolution up to 200 μm in *x-y* plane (the horizontal plane) and 50 μm in *z* direction (the vertical direction). However, the surface of precipitation printed samples is still rough due to the porous characteristic of its microstructure, which is shown by scanning electron microscope (SEM) images in Fig. 2b & c. As shown in Fig. 2b, the PVDF prints are highly porous, however, the layers of the prints are well adhered to one another and the material fills the printed volume well as seen in Fig. 2c, which indicates no layer separation. The interlayer bonding is formed by the same mechanism as solvent welding (solvent bonding), which uses a layer of solvent to soften the surface of the polymer to allow chain diffusion [27]. When printing a layer on top of another existing solid layer, the printing solution that comes out of the needle initially has a lot of solvent in it, which can partially dissolve the top surface of the lower solid layer and mix with the new half-solid layer to form interlayer bonding. Most voids are likely from porosity of the material itself due to the solvent diffusion which causes rapid polymer shrinkage and the diffusion of the solvent from the polymer. Although the diffusion of the solvent out of the PVDF solution leads to the high porosity of the prints, it is necessary to trap the solute in place for additional layer deposition.

Besides soft fluoropolymers, rigid polymers like PMMA can also be printed by this technique. Precipitation printed PMMA in the form of a wrench and chess samples are shown in Fig. 2d. Due to the porous microstructure of precipitation printed PMMA, the samples are not as transparent as commercial PMMA sheets however they do show improved structure over PVDF. Fig. 2d shows the PMMA wrench with 100 % infill density is more transparent than the two PMMA towers with 80 % infill density.

The precipitation printing technique can also be applied to 3D print polymer nanocompoites. Fig. 2e shows two 3D printed MWCNTs-PVDF nanocomposite thin-walled tubes demonstrating the high aspect ratio

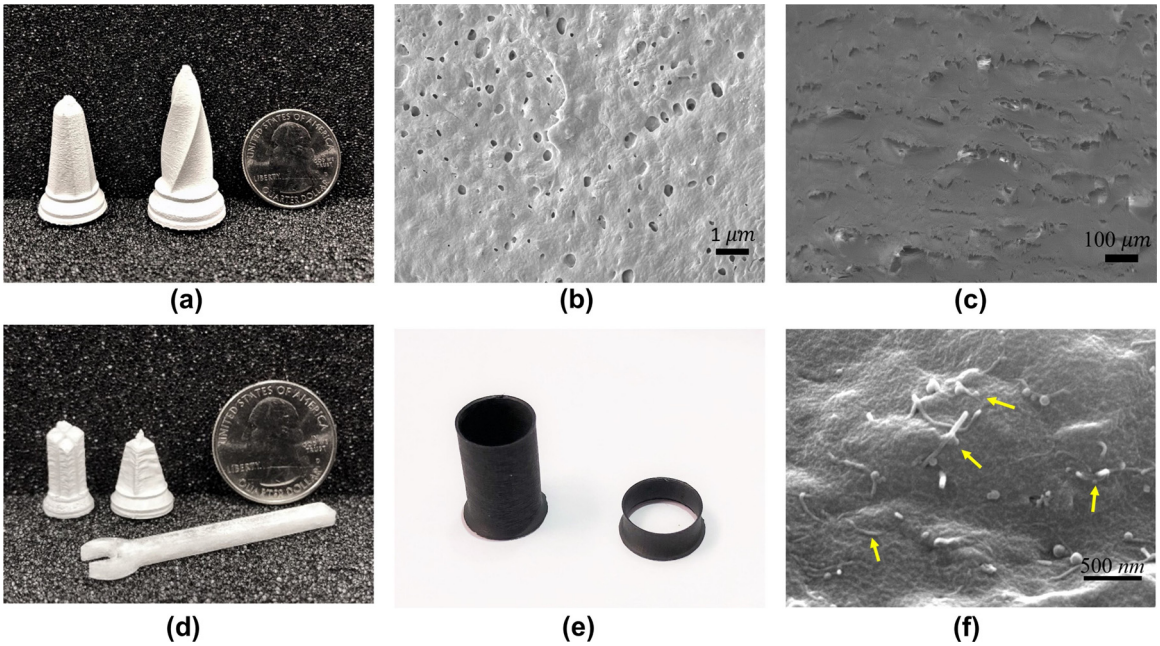

Fig. 2. (a) Printed PVDF chess structures. (b) SEM image of the porous top surface of a printed PVDF sample. (c) SEM image of a cross-section of a printed PVDF sample with a layer height of 100 μm. (d) Printed PMMA wrench and chesses. (e) Printed MWCNTs-PVDF nanocomposite thin-walled structures. (f) SEM image of the printed PVDF-MWCNTs sample (6 wt% MWCNTs).

and dimensional stability of the printing process. The nanocomposite tube can have a wall thickness of only 0.25 mm. Fig. 2f shows a SEM image of a 6 wt% MWCNTs-PVDF nanocomposite sample and as can be seen in Fig. 2f, MWCNTs are randomly dispersed in PVDF as indicated by the yellow arrows, allowing the printing of electrically conductive structures.

In addition to thermoplastics, thermoset polymers can also be printed through this technique and have been demonstrated through the printing of acrylonitrile butadiene rubber (NBR) and subsequent crosslinking through radical polymerization. Fig. 3a shows a printed "block M" which was first printed as a mixture of NBR and a latent peroxide catalyst (tert-Butyl peroxybenzoate) at room temperature and then dried in a vacuum chamber. The color of NBR before curing was cream and turned to brown after the curing process at 125 °C in an oven for 20 min to allow the tert-Butyl peroxybenzoate to form radicals beyond its decomposition temperature (SADT) of 65.8 °C [28], as shown in Fig. 3b. The precipitation technique allowed uniform mixing of the liquid catalyst (*e.g.*, peroxide) with soluble rubber enabling a uniform cross-linked structure after curing. However, although the precipitation printing technique provided high precision 3D printing for an accurately finished part, it is difficult to maintain the dimensional stability during the elevated temperature curing process. Generally, this could be avoided through the use of photoinitiator and *in situ* layer by layer photo-curing for material extrusion method, but for precipitation printing light penetration is also difficult for a submerged structure in the non-solvent.

Besides the wide range of materials to print macro-scale structures, the precipitation printing technique can also be used to print micro-scale structures with high resolution. By using a small diameter needle (30-gauge), the printing resolution could be increased up to 100 μm with a layer height of only 30 μm. The *x-y* position accuracy of the print was dictated by the positional accuracy of the gantry system, which was ± 1.5 μm. This printing resolution is higher than that of the conventional material extrusion which usually has a 100 μm layer height and poor *x-y* resolution due to the high viscosity of the polymer melt. Fig. 4a & b show a PVDF micro scaffold structure which from the SEM image can be seen to have straight scaffold structures, therefore demonstrating the high printing precision of the printing process. The printing resolution is limited by the internal diameter of the needle and therefore a finer needle will further enhance the printing resolution.

The ability of printing overhang structures without supports are shown in Fig. 5, where four inclined four prism with overhang angles

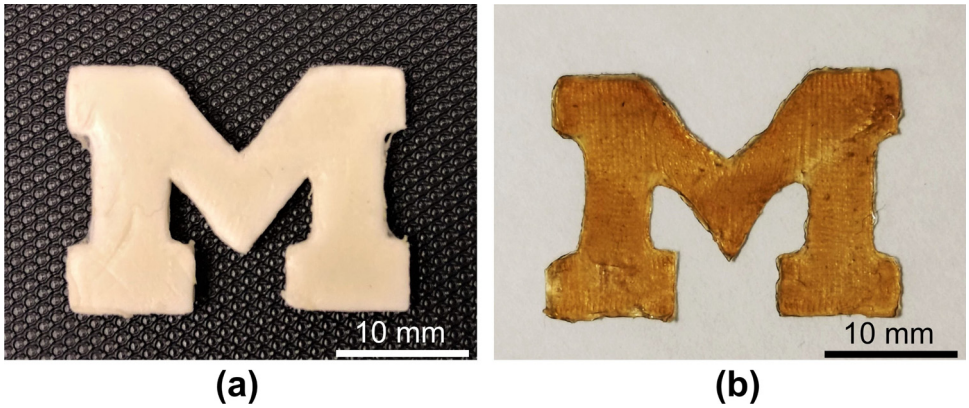

Fig. 3. (a) Printed NBR "block M" before curing. (b) Printed NBR "block M" after curing.

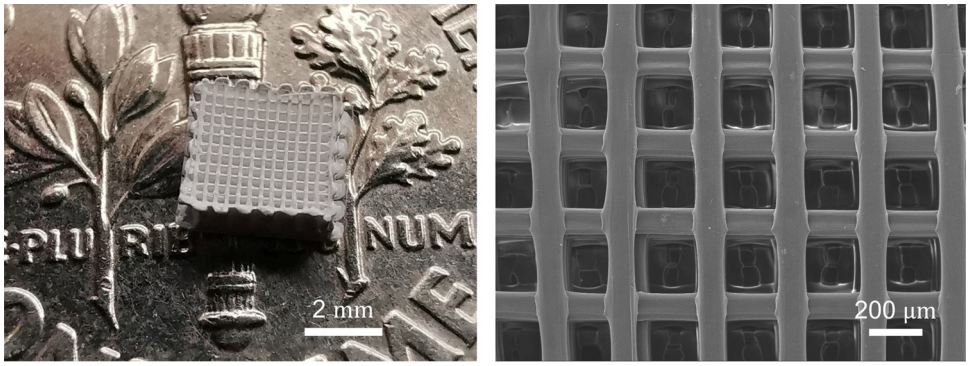

Fig. 4. (a) Micro scaffold structure on a dime coin. (b) SEM image of the scaffold structure.

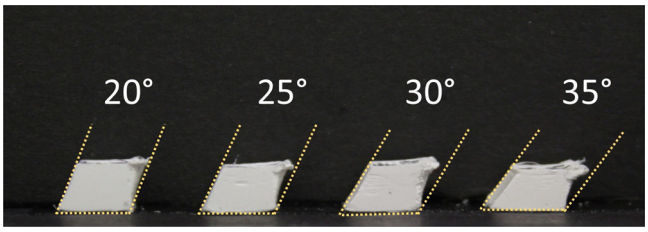

Fig. 5. Printing capability of overhang structures.

20°, 25°, 30° and 35° were made of PVDF. From the result of the prints, overhang angle less than 20° is suitable for the precipitation printing of PVDF in DMF solution. Larger than 25° overhang angles result in significant warping and shrinkage of the overhang surface. However, the overhang ability largely depends on the solvent diffusion rate in the non-solvent. If the solvent has a higher diffusion rate (*e.g.* acetone diffusing in water), the overhang angle could be further improved.

3.2. Porosity and mechanical properties tailoring

Precipitation printing utilizes the rapid diffusion of the solvent to the non-solvent reservoir to precipitate the polymer. Therefore, the removal of the solvent causes the prints to have unavoidable porosity, but this technique also allows the tailoring of the porosity and mechanical properties of the prints by controlling the printing parameters. Besides the applied pressure for solution dispensing and the viscosity of the printing ink, which were characterized by Karyappa et al. [26], the effect of different solvent/non-solvent pairs, salinity of the non-solvent and printing temperature on the porosity and mechanical properties of the prints are investigated in this research.

3.2.1. Solvent/non-solvent pairs

Different solvent/non-solvent pairs have significant difference in diffusion rate. To demonstrate the influence of solvent/non-solvent pairs on the porosity and mechanical properties, PVDF printed by DMF/water pair and PMMA printed by acetone/water pair are compared with bulk material properties. All other printing parameters, such as printing speed, pressure, and solution concentration are optimized for both polymers to get the best precipitation printed samples. Density measurements were performed on 3D printed samples of both PVDF and PMMA. The results are tabulated in Table 1 and show the density of fully filled precipitation printed PVDF is 0.646 ± 0.012 g/cm^3, which is only 36 % of fully dense commercial PVDF that has a density of 1.78 g/cm^3 [29], and is also much lower than material extrusion printed PVDF (1.51-1.67g/cm^3) reported by Porter et al. [30]. The density of fully filled precipitation printed PMMA is 1.023 ± 0.021 g/cm^3, which is 87 % of fully dense PMMA (1.18 g/cm^3) [31] and shows a much lower porosity than 3D printed PVDF due to the increased miscibility and diffusion rate between the solvent and non-solvent.

Table 1
Printed PVDF and PMMA density properties.

		PVDF	PMMA
Printing settings	Needle size	26-gauge (254 μm)	26-gauge (254 μm)
	Printing speed	7 mm/s	7 mm/s
	Layer height	0.05 mm	0.05 mm
	Extrusion width	0.2 mm	0.4 mm
	Infill percentage	100 %	100 %
	Pressure	2.5 psi (17.2 kPa)	2.0 psi (13.8 kPa)
	Solution	15 wt% PVDF in DMF	25 wt% PMMA in acetone
Density properties	Measured density	0.646g/cm^3	1.023g/cm^3
	Fully dense material density	1.78g/cm^3	1.18g/cm^3
	Density percentage	36 %	87 %

Tensile tests of the precipitation printed samples were performed with 3 different printing infill patterns: all 0° from the load axis (parallel), all 90° from the load axis (perpendicular) and 0°/ 90° alternating layer by layer. As shown in Fig. 6, the PVDF sample printed in the direction parallel to the infill pattern had the highest Young's modulus, tensile strength and tensile strain, and the PVDF sample printed in the direction perpendicular to the infill pattern had the lowest Young's modulus, tensile strength and tensile strain, while the PVDF sample printed in alternating infill direction was in between. The specimens printed in the 0° direction exhibit a high tensile strain to failure of 180 % in the direction parallel to the infill pattern was observed, which is much higher than the tensile strain when printed in the 90° direction and an alternating pattern. The stress – strain curve is shown in Fig. 6d and demonstrates a large yielding region of significantly increased strain with only slightly increasing stress which is due to the uniaxial drawing of the polymer. This indicates that the precipitation printed PVDF is compliant and plastic in the printing direction where the material is continuous. When stressed perpendicular to the infill pattern, the small voids present between adjacent tool paths leads to defects that weaken the mechanical properties of the polymer, especially for tensile strain because cracks are initiated near the voids which ultimately lead to failure prior to drawing of the polymer. The tensile strength for specimens printed in the 0° direction is approximately 4 MPa, which is significantly lower than fully dense PVDF (60 MPa) [29], however the tensile strain to failure of the precipitation printed PVDF (180 %) is higher than commercial fully dense PVDF (20 %–150 %) [29].

The 3D printed PMMA samples showed similar Young's modulus (1.2–1.4 GPa) for all infill patterns, as shown in Fig. 7a and the highest tensile strength and tensile strain occurred with 0°/90° alternating infill

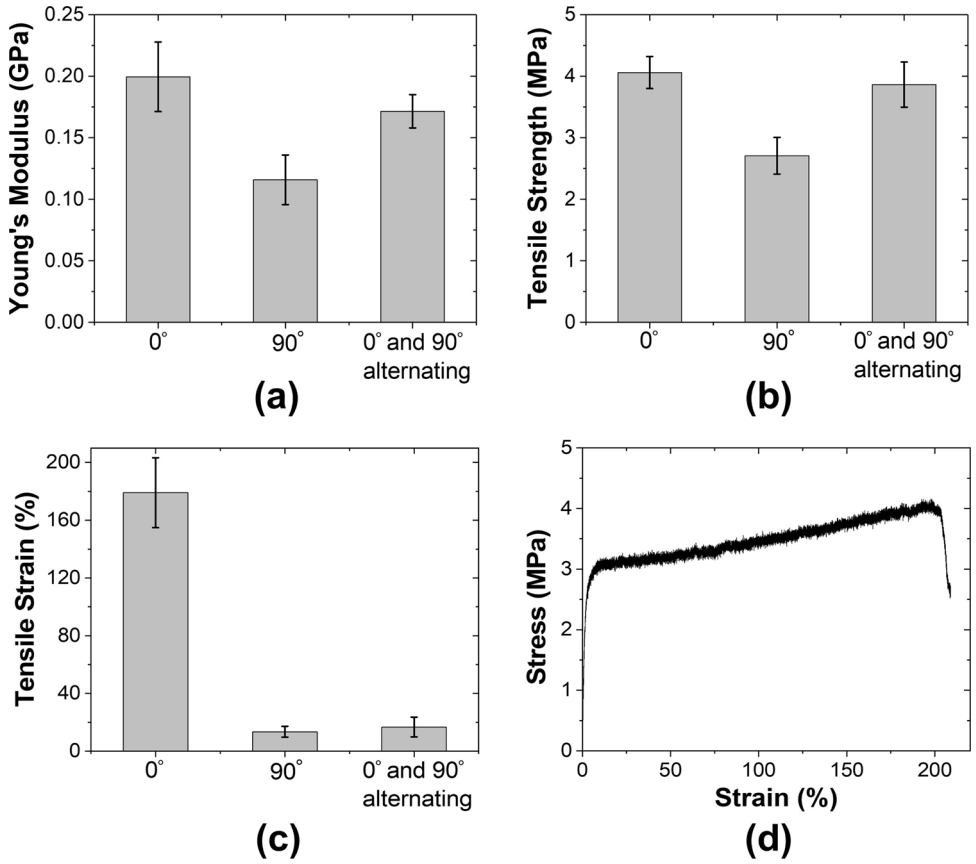

Fig. 6. Tensile test results of printed PVDF with three different infill directions. (a) Young's modulus. (b) Tensile stress. (c) Tensile strain. (d) Stress-strain curve for load axis parallel to the infill direction.

pattern, as can be seen in Fig. 7b & c. The tensile samples exhibited crack formation and subsequent failure before large scale yielding which is due to the relatively small number of voids in the printed PMMA samples and discrete interfaces between adjacent printed traces of the polymer which led to failure in a similar manor as observed in material extrusion. For samples with a 0°/90° alternating infill pattern, the upper-layer material precipitation process allowed a defect-repair process by printing directly onto the lower-layer voids. Therefore, samples with a 0°/90° alternating infill pattern had fewer defects than the samples with a 0° or 90° infill pattern, and thus demonstrated higher tensile strength and tensile strain. Among all these infill patterns, the highest Young's modulus is 1.4 GPa and the highest tensile strength is 23.3 MPa, which is lower than fully dense PMMA (3.1 GPa Young's modulus and 72 MPa tensile strength) [31]. However, compared with PMMA printing through other techniques, precipitation printed PMMA shows higher mechanical properties. For instance, material extrusion printed PMMA reported by Espalin et al. had a Young's modulus of 370 MPa and yield strength 16 MPa [32] while binder jet printed PMMA reported by Polzin et al. had a Young's modulus of 223 MPa and tensile strength 2.91 MPa [33]. This result shows that the precipitation printing technique provides a new way to 3D print polymers with high strength and stiffness. The mechanical test results of the precipitation printed PVDF showed plastic behavior while PMMA showed elastic behavior indicating the potential to tailor material properties of the 3D printed polymers by choosing different solvent-polymer pairs through the precipitation printing technique.

3.2.2. *Salinity of the non-solvent*

The solubility of the polymer in the non-solvent can be altered by varying the salinity of the non-solvent. To characterize the effect of salinity, the density of PVDF printed with DMF/water pair was examined with weight fraction of sodium chloride (NaCl) in water ranged

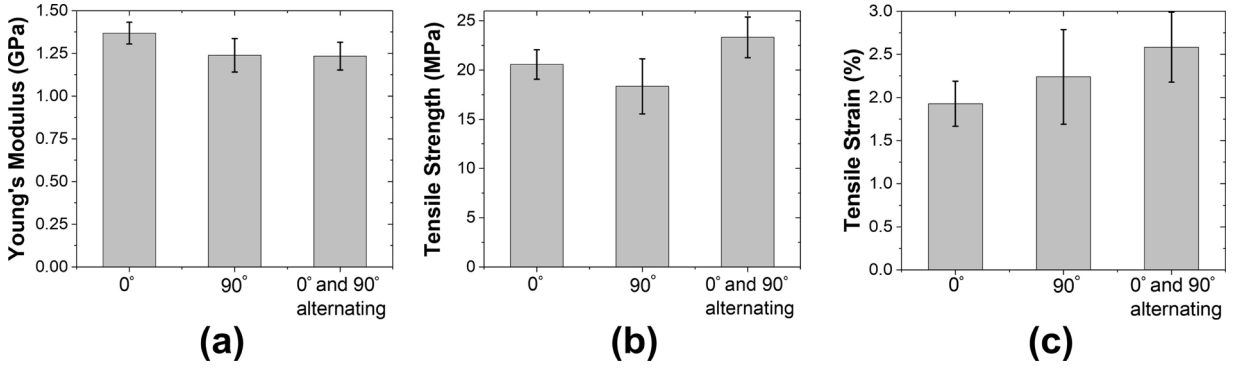

Fig. 7. Tensile test results of printed PMMA with three different infill directions. (a) Young's modulus. (b) Tensile stress. (c) Tensile strain.

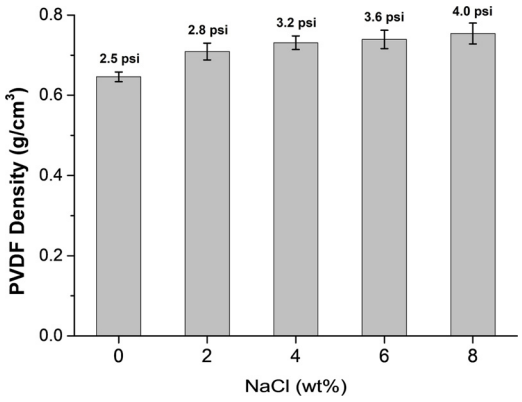

Fig. 8. Effect of salinity of the non-solvent on the printed PVDF density (printing pressure listed above each column).

from 0 to 8 wt%. By varying the salinity, the printing pressure was also adjusted to ensure the maximum infill of the prints, while other printing parameters remained the same. As shown in Fig. 8, with the increased salinity of the non-solvent, the printing pressure increased gradually, which indicates more material was printed in the same volume of the sample, and resulting in an increased density. The porosity of the PVDF prints with 8 wt% NaCl in water is 57 %, which is slightly reduced compared to the 64 % original porosity without any NaCl in water.

3.2.3. Printing temperature

The porosity of the prints mainly comes from the diffusion of the solvent trapped in the precipitated polymer to the surrounding non-solvent environment. The diffusion rate of the solvent in the non-solvent depends on temperature, which can be predicted by Stokes-Einstein equation. Experiments show that by raising the non-solvent reservoir temperature, the density of the printed PVDF with DMF/water pair increases (Fig. 9a). The printing pressure listed for each temperature was optimized to maximize the material infill in a fix volume. It should be noted that, since the viscosity of the printing solution decreases as the temperature rises, the amount of the material dispensed out of the nozzle is increased even if the pressure is set to be the same. According to the density increasement of PVDF prints with respect to the rising temperature, mechanical properties of the PVDF prints were further characterized for different printing temperatures. Fig. 9b shows the significant improvement of Young's modulus of PVDF prints with parallel infill direction, which changes from 0.20 GPa (20 °C) to 0.36 GPa (80 °C). Similar trend can be observed for tensile strength of the prints, which is increased from 4.1 MPa (20 °C) to 10.6 MPa (80 °C). Tensile test results highlight the potential of mechanical tailoring of the 3D prints by controlling the process parameters of precipitation printing.

3.3. Printed functional devices demonstration

In order to demonstrate the utility of the precipitation printing technique, several functional demonstrations are used to illustrate the broad range of polymers and devices that could be realized through this additive manufacturing method. Artificial heart replacement valves are currently in large demand for medical applications and draw a great attention to the additive manufacturing field since device performance can be maximized through a patient specific manufacturing process. The precipitation printing technique allows the printing of 3D soft valves with thermoset rubbers. In this research, NBR is used for the demonstration of a heart valve shaped 3D printed check valve. Fig. 10 shows the 3D printed check valve's closed and open state. The size of this 3D printed check valve was 15 mm in diameter and 4 mm in height. This valve allowed flow to pass in one direction when the applied pressure opened the gap automatically and blocked flow in the other direction when the gap was sealed by the applied pressure. The flow rates in two directions (direction 1: flow came from the top side, direction 2: bottom side of the check valve) at different pressures were measured to verify the effectiveness of this check valve. Fig. 11a shows the flow rate test setup with flow direction from the top side. The experiment result in Fig. 11b shows the check valve could restrict the flow rate to a low level (about 1 mL/s) from the top of the valve and it allowed flow rate to increase as the pressure rose in the other direction. According the dynamic performance of the 3D printed check valve, artificial heart replacement valves could be fabricated through precipitation printing by using biocompatible materials in the future.

Another functional application of this process is the printing of nanocomposite materials which have found use in wide ranging applications from flexible conductors to piezoelectric devices. Many nanocomposites are processed from colloidal solutions or dispersions of fillers in a solvated polymer solution which makes their printing feasible with this technique. In order to demonstrate the utility of the precipitation printing process for the realization of functional nanocomposites, electrically conductive structures have been printed using MWCNTs dispersed in a PVDF matrix. First, different weight fractions of MWCNTs in PVDF were tested to find the optimal combination of electrical conductivity as well as printing solution viscosity. Four weight fractions of MWCNTs in nanocomposites were tested: 2 wt%, 4 wt%, 6 wt% and 8 wt%, respectively. The relationship between

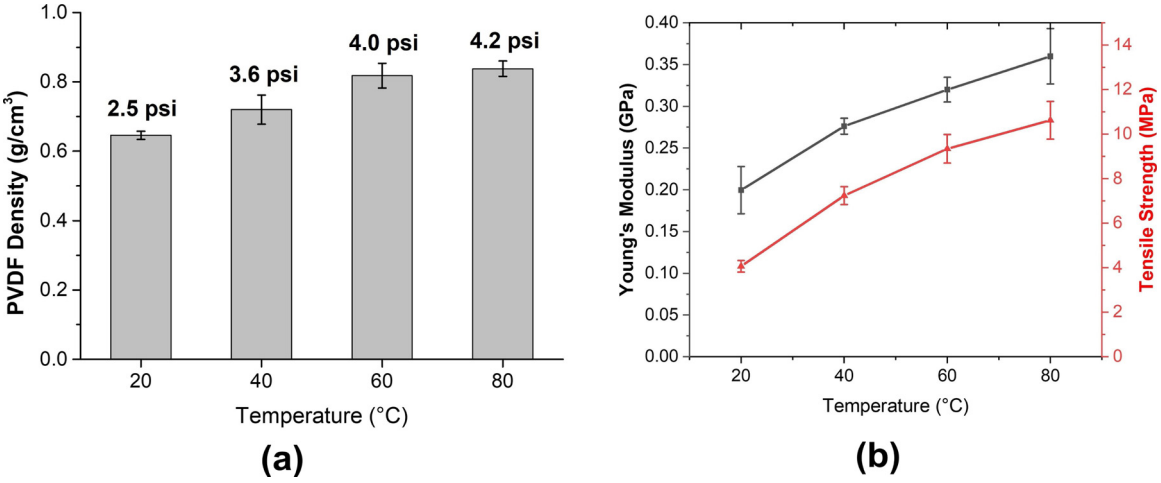

Fig. 9. (a) Influence of printing temperature on the density of PVDF prints (printing pressure listed above each column). (b) Influence of printing temperature on the mechanical properties of PVDF prints (parallel infill direction).

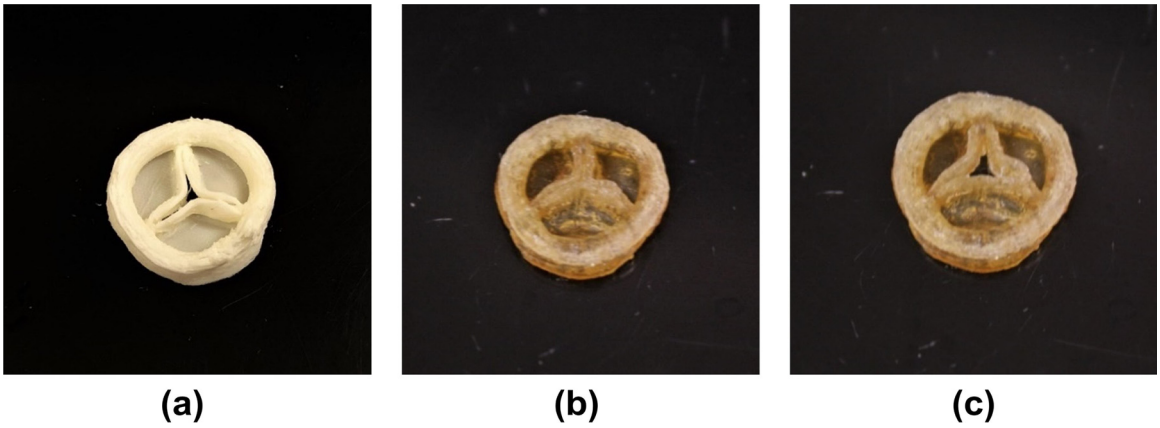

Fig. 10. 3D printed NBR check valve top view. (a) Printed valve before curing. (b) Valve's closed state after curing. (c) Valve's open state after curing.

electrical conductivity of MWCNTs-PVDF nanocomposite (measured at 1 kHz frequency) and the weight fraction of MWCNTs is shown in Fig. 12a. As reference, virgin PVDF has a negligible electrical conductivity of 10^{-9} to 10^{-8} S/m at 1 kHz frequency [34]. As can be seen in the plot, there is a rapid increase in nanocomposite electrical conductivity when MWCNTs are increased from 2 wt% to 4 wt%. While the MWCNTs-PVDF nanocomposite's electrical conductivity keeps rising as the MWCNTs weight fraction goes up, the solution becomes very viscous and prone to clogging of the nozzle when the weight fraction of MWCNTs is higher than 6 wt%. After considering the electrical conductivity and the precipitation printing process, nanocomposites with 6 wt% of MWCNTs were selected for precipitation printing. Nanocomposite of MWCNTs – PVDF has shown the potential as electrodes for piezoelectric sensors [35]. Fig. 12b shows two small 3D printed MWCNTs-PVDF nanocomposite tower structures which serve as electrodes for an LED. This demonstration showed the electrical conductivity of the 3D printed MWCNTs – PVDF nanocomposite, which had a total electrical resistance of the two structures in series to be 16 kΩ.

Carbon nanotube nanocomposites have also been shown to act as piezoresistive sensors to measure strain [36]. The piezoresistive of the precipitation printed MWCNTs-PVDF nanocomposite was measured by printing a strain gauge with a fine parallel-grid pattern to increase the accuracy of strain measurement. Fig. 13a shows the 3D printed strain gauge on Kapton tape that was coated with thin layer of PVDF applied using a doctor blade. To assess the piezoresistivity, the electrical resistance of the 3D printed strain gauge was measured under varying levels of strain from 0 to 3.0 % applied to the sample by an Instron Universal Testing Systems (Fig. 13b). The electrical resistance-strain relationship is shown in Fig. 13c and showed a trend with a linear region from 0.8 % to 2.7 % strain. The plot also shows two nonlinear regions, one at very low strains where MWCNTs inside PVDF matrix are still coiled or curled in the polymer followed by their extension and orientation and the other at larger strains followed by their slipping inside the polymer. The gauge factor (GF) was measured from the 3D printed MWCNTs-PVDF nanocomposite to assess the device sensitivity. According to test results, the printed strain gauge has a gauge factor of 1.78 that is close to commercial metallic strain gauges, which typically have a gauge factor around 2. The precipitation printing technique provides a simple and cost-efficient way to manufacture strain gauges which are capable of linearly measuring strain range from about 0.8%–2.7%. Furthermore, the conductive MWCNTs-PVDF strain gauges printed on Kapton tapes are soft and compliant, which can be easily bonded to other surfaces, even with some curvature, like gloves or human skin. The precipitation printing technique also allows for the printing of strain gauges onto existing surfaces or to be integrated into a print along with electrical traces such that a multifunctional material can be designed using additive manufacturing.

4. Conclusion

As a novel additive manufacturing method that is based on the rapid precipitation of a solvated polymer onto the part submerged in a miscible non-solvent, precipitation printing technique allows for rapid 3D printing of various materials, including thermoplastics, thermoset

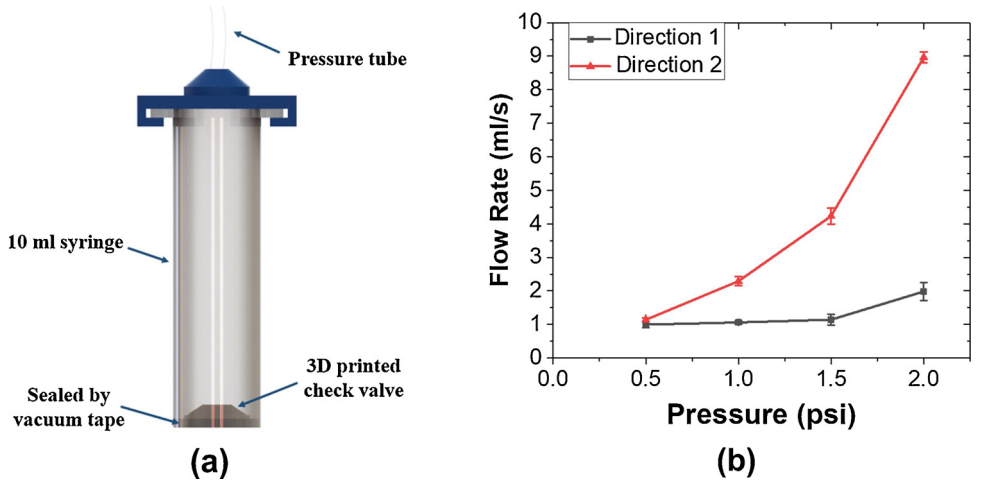

Fig. 11. (a) Flow rate test setup (flow came from the top side). (b) Flow rate - pressure relationship for two different flow directions (check valve facing up and facing down).

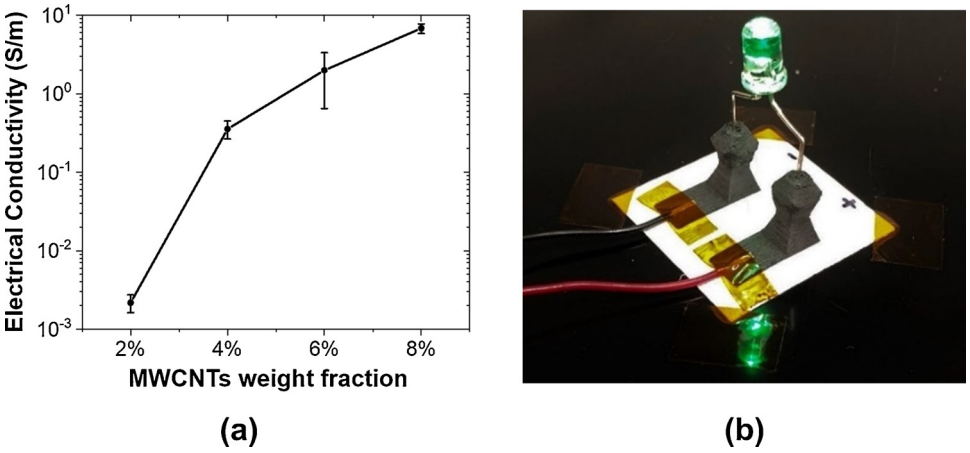

Fig. 12. (a) Electrical conductivity of 3D printed MWCNTs-PVDF nanocomposite increases as the weight fraction of MWCNTs increases. (b) Printed MWCNTs-PVDF nanocomposite tower structures serve as two electrodes of a lighted LED.

rubber and polymer nanocomposites. Precipitation printed structures are capable of achieving complex geometric shapes with a comparable size and speed of material extrusion printed structures, while printing micro-scale structures with greater than 100 μm resolution is also achievable. In addition, precipitation printing shows the potential of porosity and mechanical properties tailoring through the control of process parameters, such as solvent/non-solvent pair selection, salinity of the non-solvent and printing temperature. Among those, the solvent/non-solvent pair selection has the largest influence on the porosity tailoring since it directly affects the maximum printing solution concentration for precipitation printing. But other process parameters that influence the porosity by altering the diffusion rate among the solvent, non-solvent and polymer solute, are more practical to control during the printing to tailor material properties. With the capability of printing diverse materials and high printing resolution, precipitation printing provides a new approach to manufacture functional devices. Representative applications such as a directly printed NBR check valve and MWCNTs-PVDF strain gauge are used to demonstrate the potential of the precipitation printing process to achieve one-step additive manufacturing of functional or multifunctional devices.

5. Supplementary materials

5.1. Detailed material preparation and printing setting

5.1.1. Poly(vinylidene fluoride) (PVDF)

The printing solution was made of 15 wt% Poly(vinylidene fluoride) (PVDF) powder (Kynar 301 F, average molecular weight ~534,000) dissolved in *N,N*-dimethylformamide (DMF) (ACS certified, Fisher Chemical). The non-solvent selected to precipitate PVDF was water to ensure rapid precipitation rate due to the hydrophobic characteristic of PVDF and the high solubility of DMF in water. With a 26-gauge needle, the printing pressure was set to be 2.5 psi (17.2 kPa) and the printing speed was 7 mm/s to guarantee both printing quality and printing speed. The distance between layers (layer height) was 0.05 mm and the extrusion width was set to be 0.2 mm to avoid gaps between adjacent printing paths.

5.1.2. Poly(methyl methacrylate) (PMMA)

The printing solution was made of 25 wt% poly(methyl methacrylate) (PMMA) (Sigma-Aldrich, average molecular weight ~120,000) dissolved in Acetone (ACS reagent, Sigma-Aldrich). The non-solvent selected to precipitate PMMA was water due to the high diffusion rate of acetone to water. With a 26-gauge needle, the printing pressure was

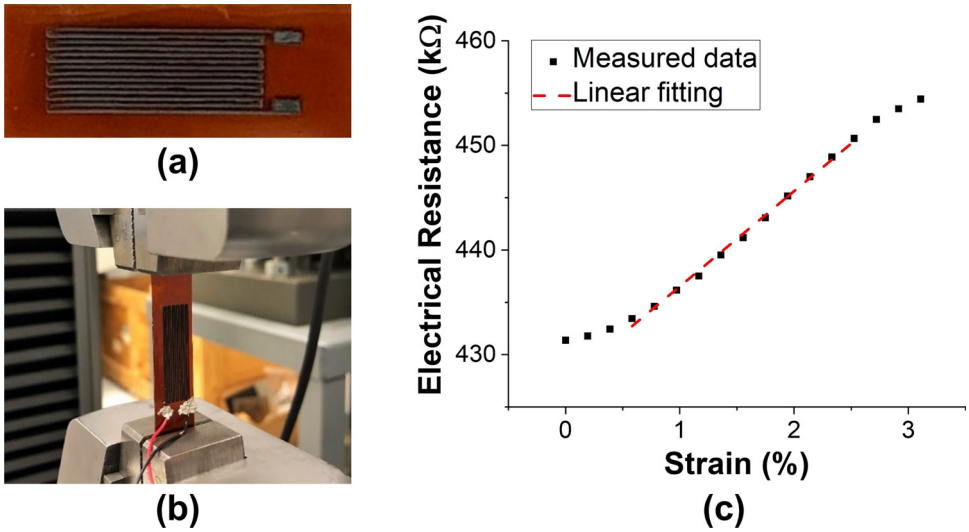

Fig. 13. (a) 3D printed strain gauge. (b) Testing printed strain gauge on an Instron Universal Testing Systems. (c) Tested electrical resistance - strain relationship of the strain gauge.

set to be 2.0 psi (13.8 kPa) and the printing speed was 7 mm/s. The layer height was 0.05 mm and the extrusion width was set to be 0.4 mm to both ensure high fill percentage and avoid overlapping of precipitated PMMA due to its rigidness.

5.1.3. Acrylonitrile butadiene rubber (NBR)

The printing solution was made of 25 wt% acrylonitrile butadiene rubber (NBR) (KUMHO PETROCHEMICAL) dissolved in *N,N*-dimethylformamide (DMF) (ACS certified, Fisher Chemical). The solution was sonicated for about 10 h to obtain a homogeneous solution. Then tert-Butyl peroxybenzoate (98 %, Alfa Aesar) was added to the printing solution, which was 2 wt% of the dissolved NBR. Since the self-accelerating decomposition temperature (SADT) of tert-Butyl peroxybenzoate is about 65.8 °C [28], premixing it with NBR would not trigger chemical reaction at room temperature. Similar to other polymers, water reservoir was used as the non-solvent for precipitation printing. Since the NBR solution is very viscous, high printing pressure that was 30.0 psi (207 kPa) and 8 mm/s printing speed were used to print with a 26-gauge needle. The layer height was 0.05 mm and the extrusion width was set to be 0.2 mm to ensure high fill percentage.

5.1.4. Multiwalled carbon nanotubes (MWCNTs) - poly(vinylidene fluoride) (PVDF) nanocomposite

The printing solution for MWCNTs-PVDF nanocomposite was selected to be 0.9 wt% MWCNTs (Cheap Tubes), 14.1 wt% PVDF (Kynar 301 F, average molecular weight ~534,000) and 85 wt% *N,N*-dimethylformamide (DMF) (ACS certified, Fisher Chemical). Thus, after the precipitation printing, MWCNTs would have a weight fraction of 6 wt% in the nanocomposite. To prepare the solution, PVDF powder was firstly dissolved into DMF by shear mixing and sonication to obtain a clear solution. Then, MWCNTs were mixed in the PVDF solution by sonication and magnetic stirring overnight to obtain a well-dispersed nanocomposite solution. To assist the dispersion process, 1 wt% of polyvinylpyrrolidone (PVP) (Sigma-Aldrich) in PVDF was also added to the solution as an emulsifier. Since PVP is miscible in water, after the precipitation, all PVP added would be removed from the final printed product. For printing process, a thin doctor blade cast PVDF film was used as the printing substrate. The printing pressure was set to be 1.4 psi (9.7 kPa) and the printing speed was 7 mm/s with a 24-gauge needle. The layer height was 0.05 mm and the extrusion width was set to be 0.2 mm to ensure high printing resolution.

5.2. Test methods

The density of printed samples was measured by 20mm × 20mm × 2mm square samples. The printing settings are listed in Table 1. The resulting prints were then fully dried under vacuum, and their dimensions were then measured with calipers to account as much as possible for any shrinking or printer errors.

Tensile tests of the printed samples with the same printing parameters for the density measurement samples were performed according to ASTM D1708 standard. This standard has been used to measure tensile properties of plastics by using microtensile specimens. Since 3D printed structures may have anisotropic properties [37], different tool path prints were tested. All 3D printed samples were 10 layers thick (0.5 mm thickness in total) and were printed with the standard specimen shape according to ASTM D1708. All deviation of the final samples from the desired dimensions was noted and accounted during Young's modulus, tensile strength and tensile strain calculations. Printed samples were tested for 3 different printing infill patterns: all 0° from the load axis (parallel), all 90° from the load axis (perpendicular) and 0°/ 90° alternating layer by layer.

Acknowledgements

The research for this paper was supported by Air Force Office of Scientific Research under contract # FA9550-16-1-0087.

References

[1] I. Gibson, D. Rosen, B. Stucker, Additive Manufacturing Technologies: 3D Printing, Rapid Prototyping, and Direct Digital Manufacturing, 2nd ed., Springer-Verlag, New York, 2015, https://doi.org/10.1007/978-1-4939-2113-3.
[2] K.V. Wong, A. Hernandez, A review of additive manufacturing, ISRN Mech. Eng. 2012 (2012) 1–10, https://doi.org/10.5402/2012/208760.
[3] I. Campbell, D. Bourell, I. Gibson, Additive manufacturing: rapid prototyping comes of age, Rapid Prototyp. J. 18 (2012) 255–258, https://doi.org/10.1108/13552541211231563.
[4] D. Bourell, J.P. Kruth, M. Leu, G. Levy, D. Rosen, A.M. Beese, A. Clare, Materials for additive manufacturing, CIRP Ann. 66 (2017) 659–681, https://doi.org/10.1016/j.cirp.2017.05.009.
[5] H. Bikas, P. Stavropoulos, G. Chryssolouris, Additive manufacturing methods and modelling approaches: a critical review, Int. J. Adv. Manuf. Technol. 83 (2016) 389–405, https://doi.org/10.1007/s00170-015-7576-2.
[6] T.D. Ngo, A. Kashani, G. Imbalzano, K.T.Q. Nguyen, D. Hui, Additive manufacturing (3D printing): a review of materials, methods, applications and challenges, Compos. Part B Eng. 143 (2018) 172–196, https://doi.org/10.1016/j.compositesb.2018.02.012.
[7] J.A. Lewis, Direct ink writing of 3D functional materials, Adv. Funct. Mater. 16 (2006) 2193–2204, https://doi.org/10.1002/adfm.200600434.
[8] F.P.W. Melchels, J. Feijen, D.W. Grijpma, A review on stereolithography and its applications in biomedical engineering, Biomaterials 31 (2010) 6121–6130, https://doi.org/10.1016/j.biomaterials.2010.04.050.
[9] S. Hashmi, G.F. Batalha, C.J.V. Tyne, B.S. Yilbas, Comprehensive Materials Processing, Elsevier, Amsterdam, 2014.
[10] K.S. Boparai, R. Singh, H. Singh, Development of rapid tooling using fused deposition modeling: a review, Rapid Prototyp. J. 22 (2016) 281–299, https://doi.org/10.1108/RPJ-04-2014-0048.
[11] W. Zhong, F. Li, Z. Zhang, L. Song, Z. Li, Short fiber reinforced composites for fused deposition modeling, Mater. Sci. Eng. A. 301 (2001) 125–130, https://doi.org/10.1016/S0921-5093(00)01810-4.
[12] F. Ning, W. Cong, J. Qiu, J. Wei, S. Wang, Additive manufacturing of carbon fiber reinforced thermoplastic composites using fused deposition modeling, Compos. Part B Eng. 80 (2015) 369–378, https://doi.org/10.1016/j.compositesb.2015.06.013.
[13] M. Nikzad, S.H. Masood, I. Sbarski, Thermo-mechanical properties of a highly filled polymeric composites for Fused Deposition Modeling, Mater. Des. 32 (2011) 3448–3456, https://doi.org/10.1016/j.matdes.2011.01.056.
[14] J.F. Christ, N. Aliheidari, A. Ameli, P. Pötschke, 3D printed highly elastic strain sensors of multiwalled carbon nanotube/thermoplastic polyurethane nanocomposites, Mater. Des. 131 (2017) 394–401, https://doi.org/10.1016/j.matdes.2017.06.011.
[15] S. Kaur, D.P. Singh, Effect of annealing temperature on dielectric behavior of PVDF thick films, AIP Conf. Proc. 1832 (2017) 120003, , https://doi.org/10.1063/1.4980688.
[16] K. Singh, Experimental study to prevent the warping of 3D models in fused deposition modeling, Int. J. Plast. Technol. 22 (2018) 177–184, https://doi.org/10.1007/s12588-018-9206-y.
[17] M.S. Alsoufi, A.E. Elsayed, Warping deformation of desktop 3D printed parts manufactured by open source fused deposition modeling (FDM) system, Int. J. Mech. Mechatron. Eng. 17 (2017) 11.
[18] S.-Z. Guo, F. Gosselin, N. Guerin, A.-M. Lanouette, M.-C. Heuzey, D. Therriault, Solvent-cast three-dimensional printing of multifunctional microsystems, Small 9 (2013) 4118–4122, https://doi.org/10.1002/smll.201300975.
[19] S. Bodkhe, G. Turcot, F.P. Gosselin, D. Therriault, One-step solvent evaporation-assisted 3D printing of piezoelectric PVDF nanocomposite structures, ACS Appl. Mater. Interfaces 9 (2017) 20833–20842, https://doi.org/10.1021/acsami.7b04095.
[20] G. Postiglione, G. Natale, G. Griffini, M. Levi, S. Turri, Conductive 3D microstructures by direct 3D printing of polymer/carbon nanotube nanocomposites via liquid deposition modeling, Compos. Part Appl. Sci. Manuf. 76 (2015) 110–114, https://doi.org/10.1016/j.compositesa.2015.05.014.
[21] D. Puppi, C. Mota, M. Gazzarri, D. Dinucci, A. Gloria, M. Myrzabekova, L. Ambrosio, F. Chiellini, Additive manufacturing of wet-spun polymeric scaffolds for bone tissue engineering, Biomed. Microdevices 14 (2012) 1115–1127, https://doi.org/10.1007/s10544-012-9677-0.
[22] C. Mota, S.-Y. Wang, D. Puppi, M. Gazzarri, C. Migone, F. Chiellini, G.-Q. Chen, E. Chiellini, Additive manufacturing of poly[(R)-3-hydroxybutyrate-co-(R)-3-hydroxyhexanoate] scaffolds for engineered bone development, J. Tissue Eng. Regen. Med. 11 (2017) 175–186, https://doi.org/10.1002/term.1897.
[23] A. Walther, J.V.I. Timonen, I. Díez, A. Laukkanen, O. Ikkala, Multifunctional high-performance biofibers based on wet-extrusion of renewable native cellulose nanofibrils, Adv. Mater. 23 (2011) 2924–2928, https://doi.org/10.1002/adma.201100580.
[24] A. Pfister, R. Landers, A. Laib, U. Hübner, R. Schmelzeisen, R. Mülhaupt, Biofunctional rapid prototyping for tissue-engineering applications: 3D bioplotting versus 3D printing, J. Polym. Sci. Part Polym. Chem. 42 (2004) 624–638, https://doi.org/10.1002/pola.10807.
[25] C. Carvalho, R. Landers, R. Mülhaupt, Soft and hard implant fabrication using 3D-BioplottingTM, (n.d.) 10.
[26] R. Karyappa, A. Ohno, M. Hashimoto, Immersion precipitation 3D printing (*ip* 3DP), Mater. Horiz. 6 (2019) 1834–1844, https://doi.org/10.1039/C9MH00730J.

[27] V.K. Stokes, Joining methods for plastics and plastic composites: an overview, Polym. Eng. Sci. 29 (1989) 1310–1324, https://doi.org/10.1002/pen.760291903.
[28] S.-Y. Cheng, J.-M. Tseng, S.-Y. Lin, J.P. Gupta, C.-M. Shu, Runaway reaction on tert-butyl peroxybenzoate by DSC tests, J. Therm. Anal. Calorim. 93 (2008) 121–126, https://doi.org/10.1007/s10973-007-8831-z.
[29] J. Inderherbergh, Polyvinylidene fluoride (PVDF) appearance, general properties and processing, Ferroelectrics 115 (1991) 295–302, https://doi.org/10.1080/00150193.1991.11876614.
[30] D.A. Porter, T.V.T. Hoang, T.A. Berfield, Effects of in-situ poling and process parameters on fused filament fabrication printed PVDF sheet mechanical and electrical properties, Addit. Manuf. 13 (2017) 81–92, https://doi.org/10.1016/j.addma.2016.11.005.
[31] U. Ali, K.J.B.A. Karim, N.A. Buang, A review of the properties and applications of poly (Methyl methacrylate) (PMMA), Polym. Rev. 55 (2015) 678–705, https://doi.org/10.1080/15583724.2015.1031377.
[32] D. Espalin, K. Arcaute, D. Rodriguez, F. Medina, M. Posner, R. Wicker, Fused deposition modeling of patient-specific polymethylmethacrylate implants, Rapid Prototyp. J. 16 (2010) 164–173, https://doi.org/10.1108/13552541011034825.
[33] C. Polzin, S. Spath, H. Seitz, Characterization and evaluation of a PMMA-based 3D printing process, Rapid Prototyp. J. 19 (2013) 37–43, https://doi.org/10.1108/13552541311292718.
[34] J.A. Puértolas, J.F. García-García, F.J. Pascual, J.M. González-Domínguez, M.T. Martínez, A. Ansón-Casaos, Dielectric behavior and electrical conductivity of PVDF filled with functionalized single-walled carbon nanotubes, Compos. Sci. Technol. 152 (2017) 263–274, https://doi.org/10.1016/j.compscitech.2017.09.016.
[35] S. Mishra, K.T. Kumaran, R. Sivakumaran, S.P. Pandian, S. Kundu, Synthesis of PVDF/CNT and their functionalized composites for studying their electrical properties to analyze their applicability in actuation & sensing, Colloids Surf. Physicochem. Eng. Asp. 509 (2016) 684–696, https://doi.org/10.1016/j.colsurfa.2016.09.007.
[36] M.A. Cullinan, M.L. Culpepper, Carbon nanotubes as piezoresistive microelectromechanical sensors: theory and experiment, Phys. Rev. B 82 (2010) 115428, , https://doi.org/10.1103/PhysRevB.82.115428.
[37] S. Ahn, M. Montero, D. Odell, S. Roundy, P.K. Wright, Anisotropic material properties of fused deposition modeling ABS, Rapid Prototyp. J. 8 (2002) 248–257, https://doi.org/10.1108/13552540210441166.